Evolving collective structures in the transitional nuclei ^{162}W and ^{164}W

D. T. Joss *et al.*

Phys. Rev. C **93**, 024307 — Published 5 February 2016

DOI: 10.1103/PhysRevC.93.024307

Evolving collective structures in the transitional nuclei ^{162}W and ^{164}W

D.T. Joss,[1] G.D. Dracoulis,[2,*] E. Higgins,[1] M. Lewis,[1] J. Thomson,[1] G.J. Lane,[2] R.D. Page,[1] J. Simpson,[3] L. Bianco,[1] B. Cederwall,[4] I.G. Darby,[1] P.M. Davidson,[2] S. Eeckhaudt,[5] S. Ertürk,[6] B. Fabricius,[2] M.B. Gómez-Hornillos,[3] T. Grahn,[5] P.T. Greenlees,[5] B. Hadinia,[4] U. Jakobsson,[5] P.M. Jones,[7] R. Julin,[5] S. Juutinen,[5] S. Ketelhut,[5] M. Leino,[5] P. Nieminen,[5] M. Nyman,[5] J. Pakarinen,[5] E.S. Paul,[1] P. Peura,[5] P. Rahkila,[5] P. Ruotsalainen,[5] M. Sandzelius,[5] P.J. Sapple,[1] J. Sarén,[5] C. Scholey,[5] J. Sorri,[5] and J. Uusitalo[5]

[1] *Oliver Lodge Laboratory, Department of Physics, University of Liverpool, Liverpool, L69 7ZE, United Kingdom.*
[2] *Department of Nuclear Physics, Research School of Physics and Engineering, Australian National University, Acton, ACT 2601, Australia.*
[3] *STFC Daresbury Laboratory, Daresbury, Warrington, WA4 4AD, United Kingdom.*
[4] *Department of Physics, Royal Institute of Technology, S-10691 Stockholm, Sweden.*
[5] *Department of Physics, University of Jyväskylä, P.O. Box 35, FI-40014, Finland.*
[6] *Nigde Universitesi, Fen-Edebiyat Falkültesi, Fizik Bölümü, Nigde, Turkey.*
[7] *Department of Nuclear Physics, iThemba LABS, P.O. Box 722, Somerset West 7129, South Africa.*

(Dated: January 8, 2016)

Excited states in the neutron-deficient nuclides $^{162}_{74}$W$_{88}$ and $^{164}_{74}$W$_{90}$ were investigated using the γ-ray spectrometer, Jurogam. A change in structure is apparent from the first rotational alignments in ^{162}W and ^{164}W, whose rotationally aligned bands are interpreted as $\nu(h_{9/2})^2$ and $\nu(i_{13/2})^2$ configurations, respectively. The level schemes have been extended using recoil (-decay) correlations with the observation of excited collective structures. Configuration assignments have been made on the basis of comparisons of the deduced aligned angular momentum, as a function of rotational frequency, with the predictions of the cranked shell model.

PACS numbers: 21.10.-k, 21.10.Re, 27.70.+q
Keywords: NUCLEAR STRUCTURE ^{162,164}W; measured E_γ, I_γ, angular correlations; deduced energy level scheme; deduced rotational alignments; cranked shell model calculations.

I. INTRODUCTION

The origin of collective phenomena in atomic nuclei and their evolution outside closed shells is a central theme in nuclear physics. The development of correlated motion as a function of nucleon number is reflected in the spectrum of low-lying states, which changes according to the number of valence nucleons. The $82 \leq N \leq 126$ shell has the longest range of nuclei where excited states can be measured experimentally. The onset of collective behavior and its interplay with the underlying single-particle structure is most apparent in the transitional regions near the closed shells. The advent of selective tagging techniques has made it possible to identify excited states in the heavy $N \lesssim 88$ nuclei where collective behavior emerges outside the $N = 82$ core.

This paper reports evidence for changes in the underlying single-particle structure between the even-even $Z = 74$ isotopes ^{162}W ($N = 88$) and ^{164}W ($N = 90$). At the predicted deformation for ^{164}W ($\beta_2 = 0.161$) [1], the proton Fermi surface lies in a region of low level density near the high-Ω $h_{11/2}$ states. The neutron Fermi surface lies close to the high-j, lowest-Ω $\nu i_{13/2}$ orbital and negative-parity orbitals originating from both the $\nu f_{7/2}$ and $\nu h_{9/2}$ subshells. The $i_{13/2}$ neutron orbital dominates the yrast spectra of the $N \geq 90$ W isotopes and excitations of one (odd-A) or two (even-A) $\nu i_{13/2}$ quasineutrons are prominent at low spin and excitation energy [2–4]. However, recent γ-ray spectroscopic studies of $N < 90$ nuclei indicate that excitations involving the negative-parity $\nu f_{7/2}$ and $\nu h_{9/2}$ states are increasingly favored at low spin in the transitional nuclei above the $N = 82$ closed shell [5–10].

II. EXPERIMENTAL DETAILS

The experiment was performed at the Accelerator Laboratory of the University of Jyväsklä, Finland. Excited states in $^{164-x}$W isotopes were populated using the ^{106}Cd(^{60}Ni,2pxn) reaction at a beam energy of 270 MeV. The target was a 1.0 mg/cm^2 thick, self-supporting ^{106}Cd foil of 96.5% isotopic enrichment. An average beam current of 4 pnA was used for ∼120 hours. Prompt γ rays were detected at the target position by the Jurogam γ-ray spectrometer [11] consisting of 43 Eurogam-type escape-suppressed germanium spectrometers [12]. The recoiling fusion-evaporation residues were separated from fission products and scattered beam by the RITU gas-filled recoil separator [13] and implanted into the double-sided silicon strip detectors (DSSD) of the GREAT spectrometer [14] at the focal plane. Recoiling nuclei were distin-

*Deceased.

guished from the residual scattered beam and radioactive decays by energy loss and (in conjunction with the DSSDs) time of flight methods using the GREAT multiwire proportional counter.

All detector signals from Jurogam and GREAT were passed to the total data readout (TDR) acquisition system [15] where they were time stamped with a precision of 10 ns to allow accurate temporal correlations between γ rays detected at the target position, recoil implants at the focal plane and their subsequent radioactive decays. These triggerless data were sorted into γ-γ matrices and γ-γ-γ cubes using GRAIN [16] and analysed with the RADWARE software packages [17].

III. RESULTS

A. Excited states in ^{164}W (N=90)

The level scheme for ^{164}W, see Fig. 1, was constructed from the analysis of 2.3×10^7 three-fold γ-ray events, detected in coincidence with a recoil implantation at the focal plane. The ground-state band (band 1) in ^{164}W was first observed by Simpson *et al.* [2] in an experiment using the POLYTESSA γ-ray spectrometer in conjunction with the Daresbury recoil separator [20]. Band 1 was established beyond the first backbend to spin and parity $I^\pi = 28^+$. Figure 2 shows typical spectra highlighting γ-ray transitions in band 1 obtained from a recoil correlated-$\gamma\gamma\gamma$ cube from this work. Band 1 is established up to an excitation energy of 9303 keV and spin (30^+), see Fig. 1. An additional decay path from the known 12^+ state to the low-spin states of band 1 has been observed.

Multipolarity assignments for the γ-ray transitions were obtained from measurements of angular intensity ratios using the directional correlations from oriented states (DCO) method [18]. Three-fold and higher coincidences were analysed to mitigate the influence of gamma-ray contaminants from other reaction channels. One or more stretched E2 gamma-ray coincidences were used to select the cascade while the remaining two transitions, if detected at 158° degrees and $\sim 90°$ (86° or 94°) Jurogam positions, were incremented into a matrix. The ratios were measured according to the relation,

$$R = \frac{I_\gamma(158°, \text{gated } 90°)}{I_\gamma(90°, \text{gated } 158°)}. \quad (1)$$

The method employed was able to discriminate between stretched quadrupole and stretched dipole transitions, yielding ratios of 0.94(9) and 0.67(14) for the 490 keV ($4^+ \to 2^+$) and the 752 keV ($7^- \to 6^+$) transitions in ^{164}W, respectively [19]. The present analysis was able to confirm the multipolarity of the strongest, uncontaminated yrast transitions that were measured in the mass-gated angular correlation analysis by Simpson *et al.* [2]. In addition, it has allowed tentative spin assignments to

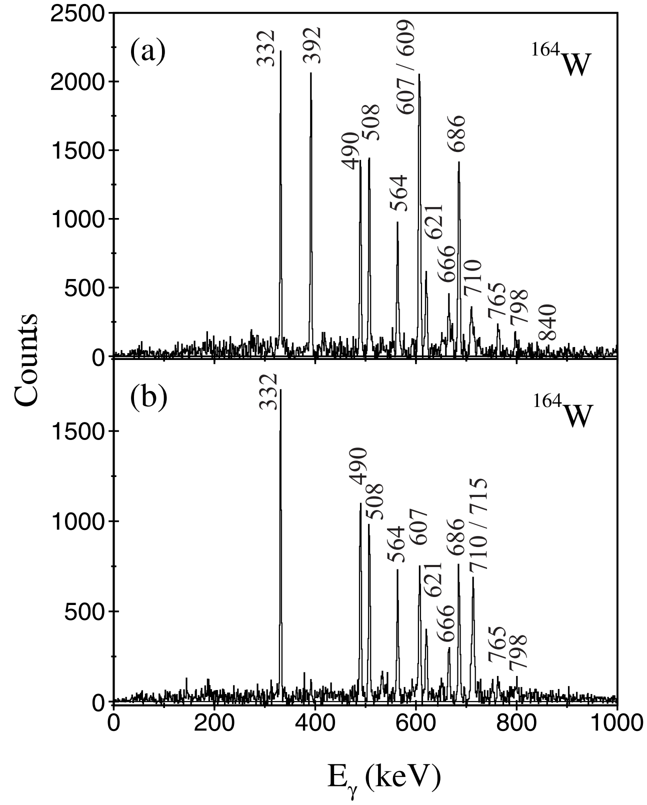

FIG. 1: Level scheme deduced for ^{164}W. The transition energies are given in keV and their relative intensities are proportional to the widths of the arrows.

be made for levels in the non-yrast structures. The properties of γ rays in ^{164}W measured in this work are listed in Table I.

Excited bands were observed in two prior studies by Hanna [19] and Dracoulis *et al.* [5]. This high-fold coincidence analysis confirms the ordering of the γ rays observed in these previous works, extending the cascades to higher spins and elucidates new decay paths to the ground state. Figure 3(a) shows a typical double-gated coincidence spectrum obtained from a recoil-$\gamma\gamma\gamma$ cube highlighting transitions in band 2 and its decay paths. Angular correlations for transitions in the decay path of band 2 to the low-spin states of band 1 are consistent with an odd-spin assignment for band 2.

Coincidence spectra showing γ rays in band 3 are shown in Fig. 3(b). A cascade of γ-ray transitions at 344, 416 and 334 keV has been observed continuing band 3 to lower spin. In addition, linking transitions at 391 and 481 keV have been observed connecting the (8^-) and (6^-) states in band 3 to band 1 via the (7^-) and (5^-) states in band 2. Two weak direct decay paths constituted by the γ rays at 1001 and 1149 keV were observed to feed the 4^+ and 2^+ states, respectively. Assuming that the linking transitions between the side bands and band 1

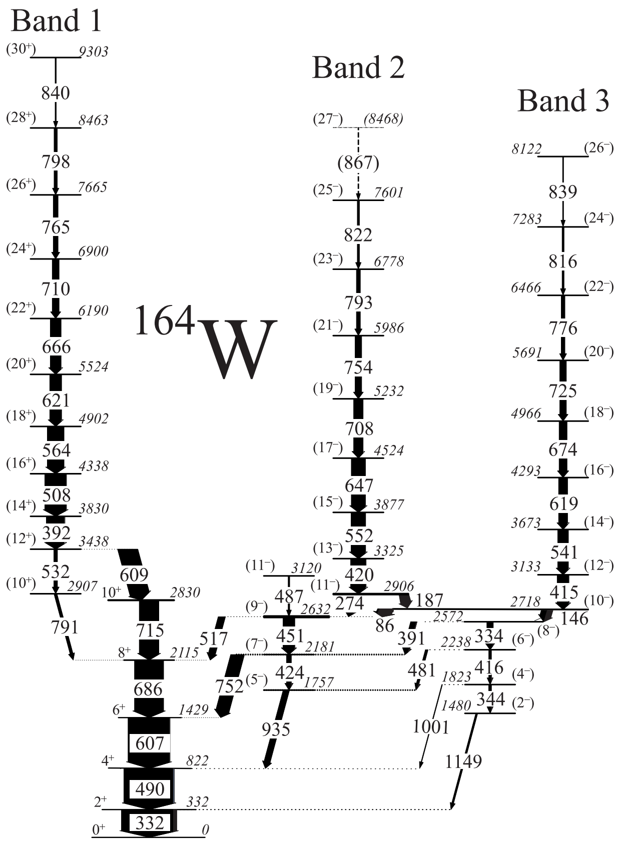

FIG. 2: Gamma-ray coincidences detected at the target position by the Jurogam spectrometer in delayed coincidence with recoils implantated in the DSSDs of the GREAT spectrometer located at the focal plane of the RITU separator (a) Summed double-gated γ-ray spectrum generated by demanding coincidences between the 715 keV transition and a list of band 1 transitions comprising the 332, 490 and 607 keV transitions. (b) Spectrum of γ rays in coincidence with the 392 keV and 609 keV transitions showing γ rays in band 1.

are electric dipoles, it has been possible to determine ratios of reduced transition probabilities by measuring the branching ratio of the interband to in-band transitions $\lambda_{\mathrm{out/in}}$, and substituting into the equation,

$$\frac{B(E1; I \rightarrow I-1)}{B(E2; I \rightarrow I-2)} = \frac{\lambda_{\mathrm{out/in}}}{1.3 \times 10^6} \frac{[E_\gamma(\Delta I = 2)]^5}{[E_\gamma(\Delta I = 1)]^3} (\mathrm{fm}^{-2}), \tag{2}$$

where γ-ray energies are given in MeV. $B(E2)$ values were estimated using the relation [21]

$$B(E2; I \rightarrow I-2) = \frac{5}{16\pi} e^2 Q_0^2 < I2K0 \mid I-2K >^2, \tag{3}$$

assuming a quadrupole moment of 4.0 eb corresponding to the predicted quadrupole deformation of $\beta_2 = 0.161$ [1]. Measured $B(E1; I \rightarrow I-1)/B(E2; I \rightarrow I-2)$ ratios are listed in Table II, together with estimated $B(E1)$ strengths.

TABLE I: Measured properties of γ ray transitions assigned to ^{164}W. Energies are accurate to ± 0.5 keV for the strong transitions ($I_\gamma > 10\%$) rising to ± 2.0 keV for the weaker transitions.

E_γ (keV)	I_γ (%)	R	$I_i^\pi \rightarrow I_f^\pi$	Band
85.8	< 2.00		$(10^-) \rightarrow (9^-)$	3→2
145.7	11.2(9)	1.3(6)	$(10^-) \rightarrow (8^-)$	3
187.4	11.2(8)		$(11^-) \rightarrow (10^-)$	2→3
273.7	16.3(11)	1.3(3)	$(11^-) \rightarrow (9^-)$	2
331.9	100.0(6)	0.8(1)	$2^+ \rightarrow 0^+$	1
334.0	11.7(10)		$(8^-) \rightarrow (6^-)$	3
343.6	5.0(8)		$(4^-) \rightarrow (2^-)$	3
391.0	10.7(11)		$(8^-) \rightarrow 7^-$	3→2
391.9	34.6(23)		$(14^+) \rightarrow (12^+)$	1
414.6	22.0(16)		$(12^-) \rightarrow (10^-)$	3
415.5	4.9(7)		$(6^-) \rightarrow (4^-)$	3
419.7	28.9(19)		$(13^-) \rightarrow (11^-)$	2
424.4	9.0(8)		$(7^-) \rightarrow (5^-)$	1
451.0	22.1(16)		$(9^-) \rightarrow (7^-)$	1
480.9	4.7(7)		$(6^-) \rightarrow (5^-)$	3→2
487.3	2.9(8)		$(11^-) \rightarrow (9^-)$	1
490.4	95(6)	0.9(1)	$4^+ \rightarrow 2^+$	1
508.0	41(3)		$(16^+) \rightarrow (14^+)$	1
517.4	13.5(10)		$(9^-) \rightarrow (8^+)$	2→1
531.6	6.8(7)		$(12^+) \rightarrow (10^+)$	1
540.5	20.1(14)		$(14^-) \rightarrow (12^-)$	3
551.7	27.5(19)		$(15^-) \rightarrow (13^-)$	2
564.1	31.7(21)		$(18^+) \rightarrow (16^+)$	1
606.6	80(5)	0.8(1)	$6^+ \rightarrow 4^+$	1
608.9	37(3)		$(12^+) \rightarrow 10^+$	1
619.1	17.0(13)		$(16^-) \rightarrow (14^-)$	3
621.4	22.5(16)		$(20^+) \rightarrow (18^+)$	1
647.2	26.9(18)		$(17^-) \rightarrow (15^-)$	2
666.3	20.5(15)		$(22^+) \rightarrow (20^+)$	1
673.8	15.1(11)		$(18^-) \rightarrow (16^-)$	3
686.0	55(4)	1.7(4)	$8^+ \rightarrow 6^+$	1
707.6	18.0(13)		$(19^-) \rightarrow (17^-)$	2
710.4	13.1(10)		$(24^+) \rightarrow (22^+)$	1
714.7	37(3)	1.2(2)	$10^+ \rightarrow 8^+$	1
724.6	12.5(10)		$(20^-) \rightarrow (18^-)$	3
751.9	25.6(21)	0.7(1)	$7^- \rightarrow 6^+$	2→1
753.7	12.5(11)		$(21^-) \rightarrow (19^-)$	2
764.6	9.2(8)		$(26^+) \rightarrow (24^+)$	1
775.5	7.0(7)		$(22^-) \rightarrow (20^-)$	3
791.0	5.6(11)		$(10^+) \rightarrow (8^+)$	1
792.6	7.5(7)		$(23^-) \rightarrow (21^-)$	2
798.3	6.1(6)		$(28^+) \rightarrow (26^+)$	1
816.4	3.7(5)		$(24^-) \rightarrow (22^-)$	3
822.4	4.1(5)		$(25^-) \rightarrow (23^-)$	2
839.3	1.8(4)		$(26^-) \rightarrow (24^-)$	3
840.1	2.1(4)		$(30^+) \rightarrow (28^+)$	1
867.1	1.7(4)		$(27^-) \rightarrow (25^-)$	2
935.3	11.9(15)		$(5^-) \rightarrow (4^+)$	2→1
1001.2	1.3(4)		$(4^-) \rightarrow 4^+$	3→1
1148.5	3.6(15)		$(2^-) \rightarrow 2^+$	3→1

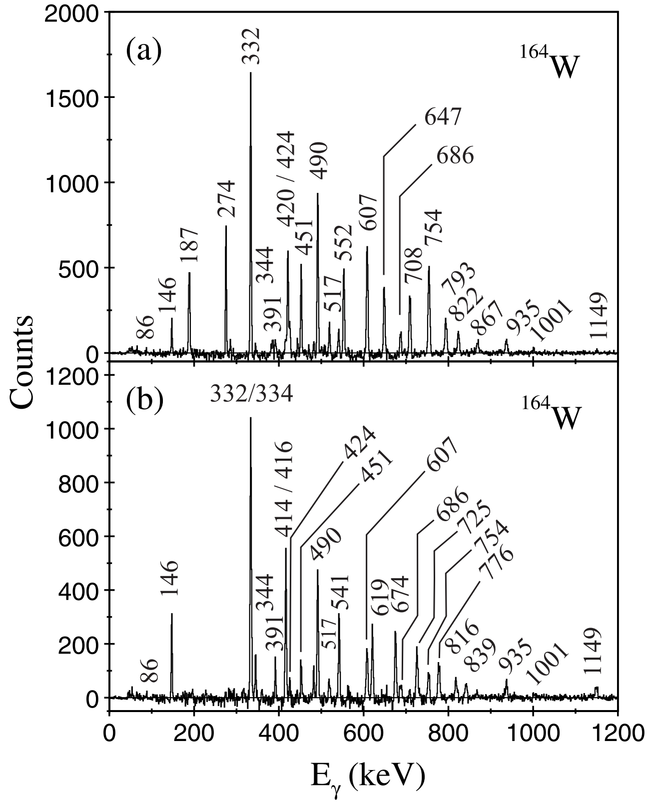

FIG. 3: Gamma-ray coincidences detected at the target position by the Jurogam spectrometer in delayed coincidence with recoils implantated in the DSSDs of the GREAT spectrometer located at the focal plane of the RITU separator. (a) Summed double-gated γ-ray spectrum generated using a list of band 2 transitions comprising the 420, 552, 647, 708, 754, 793 and 822 keV transitions. (b) Summed double-gated γ-ray spectrum generated using a list of band 2 transitions comprising the 415, 541, 619, 674, 725, 776 and 816 keV transitions.

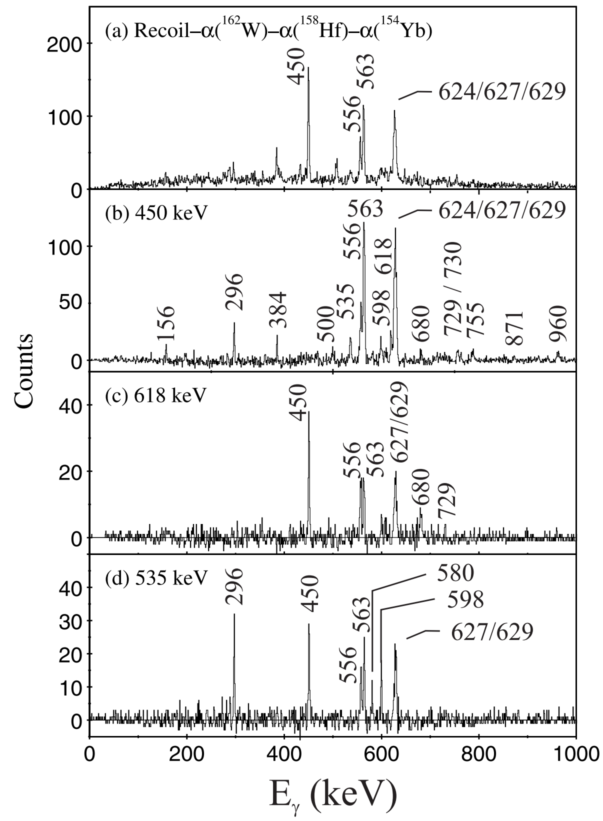

FIG. 4: Gamma rays correlated with recoil implantations followed by the characteristic decay sequence $\alpha(^{162}$W)-$\alpha(^{158}$Hf-$\alpha(^{154}$Yb) within the same DSSD pixel of the GREAT spectrometer. The correlation time was limited to 3600 ms for the first decay and 9000 ms for the second decay and 1300 ms for the third decay for this spectrum. (b) Gamma rays in coincidence with the 450 keV transition generated from an $\alpha(^{162}$W)-correlated $\gamma\gamma$ coincidence matrix. (c) Gamma rays in coincidence with the 618 keV transition generated from the same matrix. (d) Gamma rays in coincidence with the 535 keV transition generated from the same matrix. The time for recoil-decay correlations was limited to the range 500–4800 ms for the spectra in panels (b), (c) and (d). Gamma-ray transitions in the ground-state band of ^{162}W are labelled by their energy in keV.

TABLE II: Experimental $B(E1)/B(E2)$ ratios of reduced transition probabilities and deduced $B(E1)$ strengths in ^{164}W. The $B(E2)$ values were estimated using the predicted deformation parameters in Ref [1].

I	E_x (keV)	$\frac{I_\gamma(E1)}{I_\gamma(E2)}$	$\frac{B(E1)}{B(E2)}$ (10^{-7} fm^{-2})	$B(E1)$ (10^{-3} e^{2}fm^2)	$E_\gamma(E1)$ (keV)
(9)	2632	0.55(10)	0.57(11)	0.27(5)	517
(7)	2181	3.37(12)	0.83(30)	0.40(14)	752
(4)	1823	0.23(10)	0.008(4)	0.004(2)	1001

B. Excited states in ^{162}W ($N = 88$)

The yrast states in ^{162}W were first observed in experiments by Dracoulis *et al.* using the HERA and CAESAR spectrometers [5]. It has been possible to confirm the identification of γ rays in ^{162}W [10, 22] by the application of the recoil-decay tagging (RDT) technique [23–25]. The RDT technique allows spatial and temporal correlations between γ rays detected at the target position with the subsequent radioactive decays of recoiling fusion products implanted at the focal plane of a recoil separator. This method can provide an unambiguous identification of γ rays to a specific nucleus. The optimal conditions for RDT studies are realised for nuclei with short radioactive decay half-lives, high α-decay branching ratios and a distinctive decay energy. Ideally, the implantation rate should be low in comparison with the half-life of the 'tagging' decay, i.e. no greater than one implantation every 3-5 half-lives. If two ions impinge on a pixel in a time comparable with the half-life, a random correlation

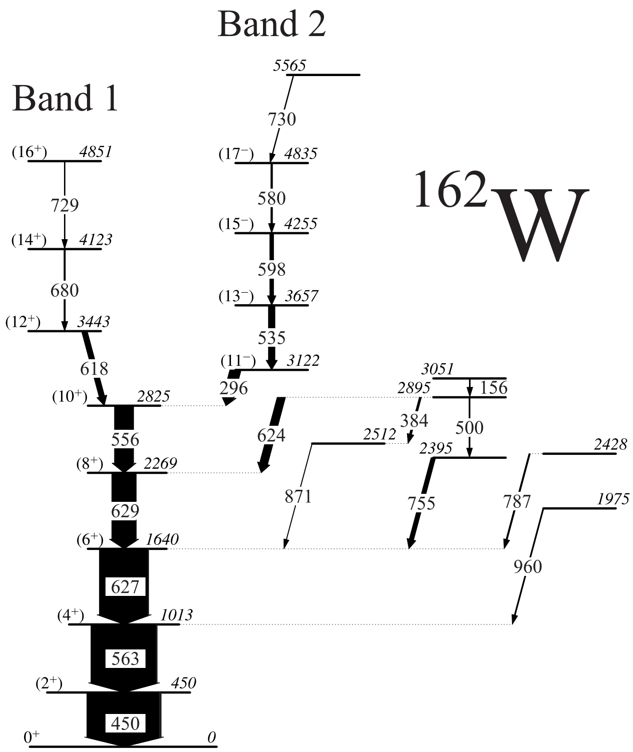

FIG. 5: Level scheme deduced for ^{162}W. The transition energies are given in keV and their relative intensities are proportional to the widths of the arrows.

will occur rendering an unreliable identification. Error weighted average decay properties obtained from previous α-decay measurements of ^{162}W (E_α = 5536(3) keV, $t_{1/2}$ = 1364(37)ms, b_α=49.4(18)%) [26–29] suggest that an unambiguous recoil-decay correlation can be achieved at the average recoil rate 1.4 kHz (or $\sim$ 1 per pixel per second) employed in this experiment.

Figure 4(a) shows γ rays correlated with a recoil implanted in the GREAT spectrometer followed by the characteristic α decays of ^{162}W and those of its subsequent daughter (^{158}Hf) and granddaughter (^{154}Yb) detected within the same pixel. The correlation times between implantation and the subsequent decays was limited to 3600 ms, 9000 ms and 1300 ms, respectively. These recoil decay correlations reproduce the ground-state band in ^{162}W (band 1) observed in references [5, 10, 22].

The remaining panels in Fig. 4 show typical coincidence spectra tagged with the α(^{162}W) decay. Recoil-decay correlations were limited to the period 500-4800 ms following an implantation within the same DSSD pixel. The matrix contained 6$\times$10^5 α-correlated $\gamma\gamma$ events. This search time was chosen to eliminate the background from shorter lived channels populated strongly in the reaction. The same correlation conditions were used to produce angular correlation matrices. The level scheme deduced from this work is shown in Fig. 5 and the properties of γ rays in ^{162}W are listed in Table III.

TABLE III: Measured properties of γ-ray transitions assigned to ^{162}W. Energies are accurate to $\pm$0.5 keV for the strong transitions (I_γ >10%) rising to $\pm$2.0 keV for the weaker transitions.

E_γ (keV)	I_γ (%)	R	$I_i^\pi \rightarrow I_f^\pi$	Band
156.1	4.2(7)			
295.9	15.0(13)		$(11^-) \rightarrow (10^+)$	2→1
384.0	2.8(7)			
449.6	100.0(15)	1.2(2)	$(2^+) \rightarrow (0^+)$	1
499.8	1.5(6)			
535.0	9.0(9)		$(13^-) \rightarrow (11^-)$	2
556.2	26.1(18)		$(10^-) \rightarrow (8^+)$	1
562.8	90.0(6)	1.3(2)	$(4^+) \rightarrow (2^+)$	1
579.6	2.3(5)		$(17^-) \rightarrow (15^-)$	2
598.4	5.3(7)		$(15^-) \rightarrow (13^-)$	2
618.4	7.6(10)		$(12^+) \rightarrow (10^+)$	1
624.3	11.2(12)		$\rightarrow (8^+)$	
626.6	67(4)		$(6^+) \rightarrow (4^+)$	1
629.1	33.5(24)		$(13^-) \rightarrow (11^-)$	1
680.4	2.0(5)		$(8^+) \rightarrow (6^+)$	1
728.6	1.1(4)		$(16^+) \rightarrow (14^+)$	1
730.4	1.1(4)		$\rightarrow (17^-)$	
755.3	6.2(11)		$\rightarrow (6^+)$	
787.4	2.0(7)		$\rightarrow (6^+)$	
870.5	0.7(6)		$\rightarrow (6^+)$	
960.4	1.6(8)		$\rightarrow (4^+)$	

Figure 4(b) shows the γ rays in coincidence with the 450 keV $2^+ \rightarrow 0^+$ transition in ^{162}W. The band based on the ground state, band 1, dominates the spectrum although there is clear evidence of links to other structures. Figure 4(c) shows coincidences with the 618 keV transition that shows γ rays in band 1, which extend to $I^\pi = (16^+)$. An excited band structure, band 2, is observed to decay to the 10^+ state in band 1 via a 296 keV transition, see Fig. 4(d). It has not been possible to assign the multipolarity of the 296 keV transition in this work.

IV. DISCUSSION

In order to identify the underlying orbital configurations of the bands in ^{162}W and ^{164}W, Woods-Saxon cranking calculations have been performed [30, 31]. Quasiparticle Routhians, e' as a function of rotational frequency calculated for ^{164}W are displayed in Fig. 6. The quasiparticle Routhians are labeled according to the convention listed in Table IV. The deformation parameters (β_2=0.161, β_4=0.010) used in the cranking calculations are the values predicted in reference [1].

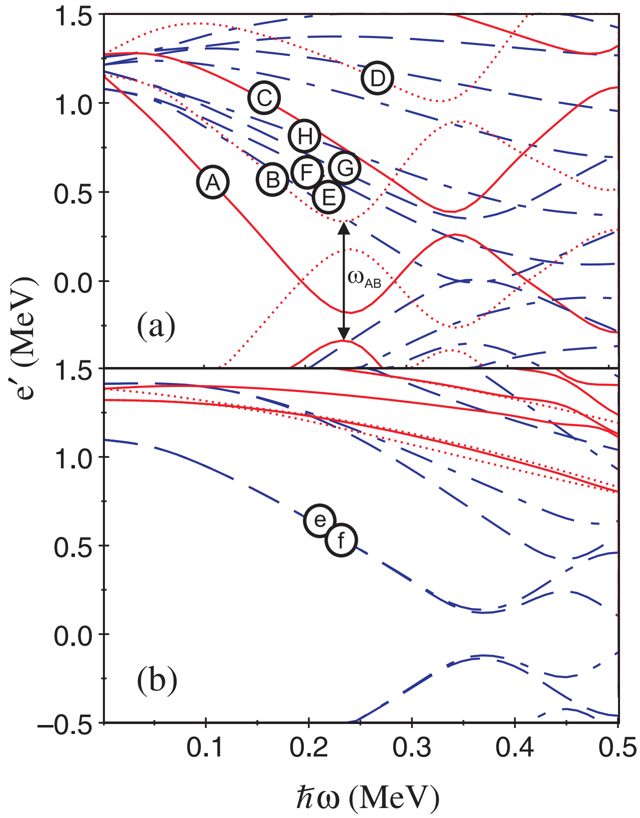

FIG. 6: (Color online) Representative cranked shell model Routhians calculated using a Woods-Saxon potential for ^{164}W. The calculations assume deformation parameters (β_2 = 0.161, β_2 = 0.010,γ=0°) from reference [1]. (a) Quasineutron Routhians plotted as a function of rotational frequency. (b) Quasiproton Routhians plotted as a function of rotational frequency.

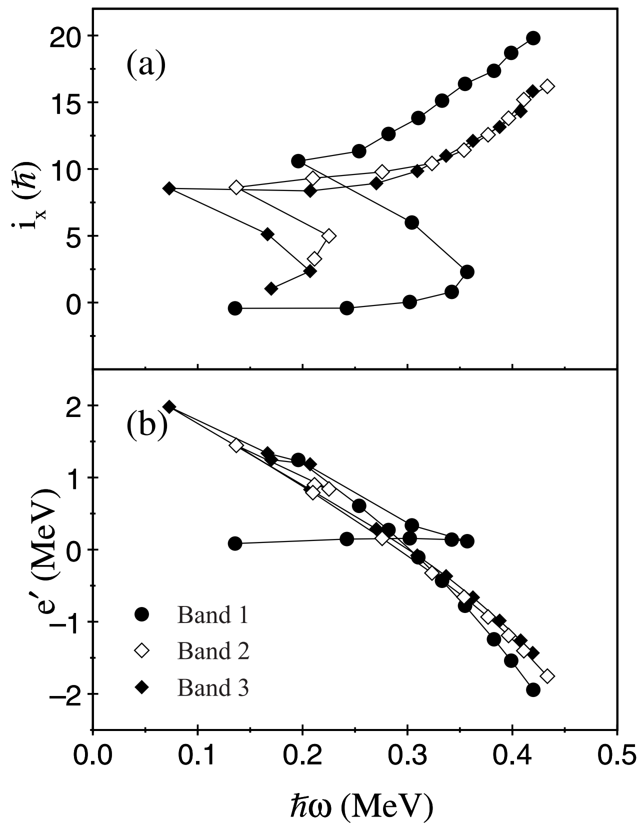

FIG. 7: The alignment, i_x as a function of rotational frequency for the bands in ^{164}W. A rotational reference, based on a configuration with a variable moment of inertia defined by the Harris parameters $\mathcal{J}_0$= 12.5 $\hbar^2$MeV^{-1} and $\mathcal{J}_1$=60 $\hbar^4$MeV^{-3}, has been subtracted from each band. (b) Experimental routhians e' as a function of rotational frequency for the bands in ^{164}W.

TABLE IV: Adopted convention for labelling quasiparticle routhians.

Label	Parity & Signature (π,α)	Shell Model State at $\hbar\omega = 0$
	Quasineutrons	
A	$(+,+1/2)_1$	$i_{13/2}$
B	$(+,-1/2)_1$	$i_{13/2}$
E	$(-,+1/2)_1$	$h_{9/2}, f_{7/2}$
F	$(-,-1/2)_1$	$h_{9/2}, f_{7/2}$
G	$(-,+1/2)_2$	$h_{9/2}, f_{7/2}$
H	$(-,-1/2)_2$	$h_{9/2}, f_{7/2}$
	Quasiprotons	
e	$(-,+1/2)_1$	$h_{11/2}$
f	$(-,-1/2)_1$	$h_{11/2}$

Experimental rotational alignments [32], i_x, as a function of rotational frequency, $\hbar\omega$, have been deduced and are compared with the predictions of the cranked shell model. Figure 7(a) shows the alignments for the bands in ^{164}W. Band 1 shows an alignment gain of $\Delta i_x = 11\hbar$ at $\hbar\omega$=0.3 MeV. The quasineutron and quasiproton Routhians shown in Fig. 6 suggest that the high-j, low-Ω $i_{13/2}$ quasineutron orbitals (A and B) are the first to undergo a rotational alignment at $\hbar\omega \sim 0.24$ MeV. The predicted alignment gain from Fig. 6 for the $i_{13/2}$ quasineutron pair (AB) is expected to be $\Delta i_x = 10.6\hbar$, which is in excellent agreement with the experimental value measured for band 1. Therefore the crossing is consistent with the $(i_{13/2})^2$ (AB) alignment as discussed previously [2]. The discrepancy of the predicted and experimental crossing frequencies is not unexpected due to the sensitivity of the calculations to the deformation and pairing input parameters.

The alignments extracted for bands 2 and 3 have similar behavior as a function of rotational frequency. At low frequency, the alignments for both bands are low but quickly achieve an alignment of $\sim 9\hbar$ at 0.2 MeV. This alignment is consistent with a two-quasiparticle configuration. However, it is lower than the alignment observed for the $(i_{13/2})^2$ (AB) configuration. The next available two-quasineutron excitations are based on coupling a single $i_{13/2}$ quasineutron to one of the nearby negative-parity orbitals originating from the mixed $f_{7/2}, h_{9/2}$ configurations. The cranking calculations predict an alignment of $\sim 9.5\hbar$ for the AE and AF configurations. Therefore, bands 2 and 3 are based on the $\nu i_{13/2} \otimes \nu(f_{7/2}, h_{9/2})$ (AE and AF) configurations. The smooth alignment gain at higher frequencies is similar for all the aligned configurations suggesting a common physical origin. This is interpreted as the gradual alignment of the $\pi(h_{11/2})^2$ (e and f) quasiprotons occurring with a large interaction strength [2].

The alignment properties for bands 2 and 3 at $\hbar\omega < 0.3$ are consistent with octupole excitations [33–38]. This assignment is supported by the large estimated $B(E1)$ reduced transition probabilities listed in Table II. Octupole excitations are expected to arise from interactions between orbitals near the Fermi surface that differ in orbital angular momentum by $\Delta l = 3$ [39]. In this region, octupole correlations are expected to arise from the $h_{11/2}$ and $d_{5/2}$ proton and $i_{13/2}$ and $f_{7/2}$ neutron orbitals.

The $N = 88$ isotone ^{162}W displays different features in the rotational alignment of its ground-state band (band 1). Figure 8(a) compares the alignment as a function of rotational frequency for bands in ^{162}W and ^{164}W. A crossing in band 1 of ^{162}W is observed at a crossing frequency of $\sim$0.3 MeV, see Fig. 8(b), which is the same as in the yrast band of ^{164}W but with a lower alignment gain ($\sim 6\hbar$). This has been interpreted in terms of the rotational alignment of a pair of $h_{9/2}$ neutrons favored by the lower average deformation of ^{162}W relative to ^{164}W [5, 6, 10]. This is the same transition between neutron configurations as observed between the neighboring $N = 88$ and $N = 90$ Ta isotones, ^{161}Ta [7] and ^{163}Ta [22]. There is a smooth increase in alignment above the backbend, which is interpreted as arising from the alignment of the $\pi(h_{11/2})^2$ quasiprotons occurring with a strong interaction strength as observed in the heavier isotope ^{164}W.

Band 2 in ^{162}W is measured to have an alignment of $\Delta i_x = 9\hbar$ at 0.3 MeV/$\hbar$, which is lower than expected for an aligned $\nu(i_{13/2})^2$ configuration. However, the degree of alignment is similar to that achieved by the $\nu i_{13/2} \otimes \nu(f_{7/2}, h_{9/2})$ configurations in ^{164}W. Thus band 2 is assigned to be a negative-parity odd-spin structure formed by the $\nu i_{13/2} \otimes (f_{7/2}, h_{9/2})$ (AE) two-quasiparticle configuration.

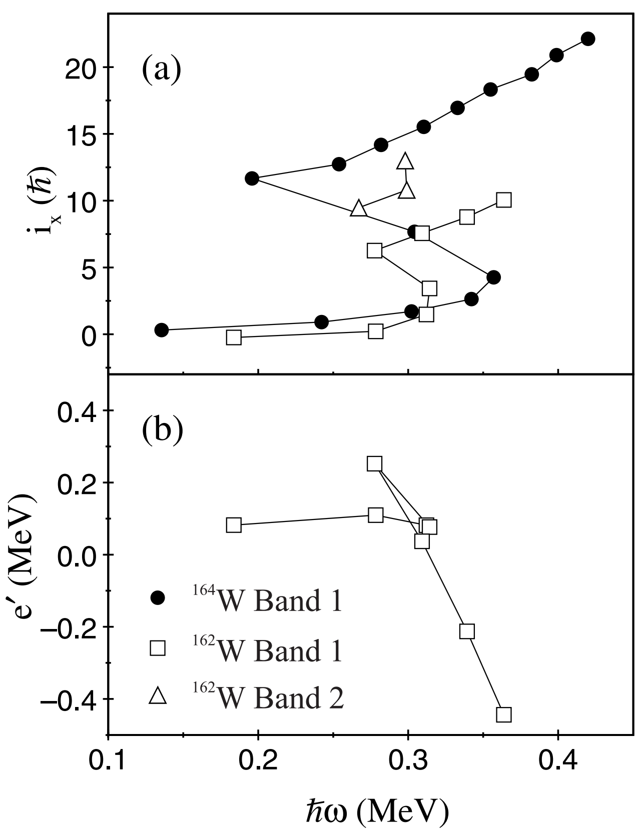

FIG. 8: (a) The alignment, i_x as a function of rotational frequency for the bands in ^{162}W and band 1 in ^{164}W. A rotational reference, based on a configuration with a variable moment of inertia defined by the Harris parameters $\mathcal{J}_0 = 7\ \hbar^2\text{MeV}^{-1}$ and $\mathcal{J}_1 = 60\ \ \hbar^4\text{MeV}^{-3}$, has been subtracted from each band. (b) Experimental routhians e' as a function of rotational frequency for the bands in ^{162}W.

V. CONCLUSION

Energy level schemes have been extended in the transitional nuclei ^{162}W and ^{164}W. The positive-parity zero and two-quasiparticle bands and the negative-parity two-quasiparticle bands have been elucidated in both isotopes using the Jurogam and GREAT spectrometers in conjunction with the RITU gas-filled separator. Configuration assignments for the bands have been assigned on the basis of the rotational alignments as a function of rotational frequency and comparisons with the predictions of the cranked shell model. These results confirm that the $\nu f_{7/2}, h_{9/2}$ states are favored over the $\nu i_{13/2}$ quasineutron configuration in forming the first rotational alignment in the ground-state band of ^{162}W. This indicates a change in the relative positions of the $f_{7/2}, h_{9/2}$ and $i_{13/2}$ neutron orbitals between $N = 88$ and $N = 90$, which is attributed to the lower deformation of the lighter isotope. The excited collective structures are interpreted as two-quasineutron $\nu f_{7/2}, h_{9/2} \otimes \nu i_{13/2}$ configurations.

VI. ACKNOWLEDGMENTS

The authors would like to acknowledge J. Burde, M.A. Deleplanque, A.O. Macchiavelli, J. Oliviera and

F.S. Stephens for kindly sharing information related to their work on ^{162}W from experiments with the HERA spectrometer at the Lawrence Berkeley National Laboratory. The authors would like to express their gratitude to the staff of the Accelerator Laboratory at the University of Jyväskylä for their excellent technical support. The authors also thank Paul Morrall of Daresbury Laboratory for the preparation of the Cd targets. Financial support for this work has been provided by the UK Science and Technology Facilities Council (STFC), the EU 6th Framework Programme, Integrating Infrastructure Initiative - Transnational Access, (EURONS, Contract No. 506065), the Academy of Finland under the Finnish Centre of Excellence Programme 2006 - 2011, and by the Swedish Research Council. K.L. would like to acknowledge the support of the Royal Society. P.T.G, C.S. and P.N. acknowledge the support of the Academy of Finland (Contract Nos. 111965, 209430 and 121110). We thank the UK/France (STFC/IN2P3) Loan Pool and the GAMMAPOOL European Spectroscopy Resource for the loan of detectors for Jurogam.

---

[1] P. Möller, J.R. Nix, W.D. Myers, and W.J. Swiatecki, Atomic Data and Nuclear Data Tables **59**, 297 (1995).
[2] J. Simpson *et al.*, J.Phys. **G17**, 511 (1991).
[3] J. Simpson *et al.*, J. Phys. **G18**, 1207 (1992).
[4] K. Theine *et al.*, Nucl. Phys. **A548**, 71 (1992).
[5] G.D. Dracoulis *et al.*, *P*roceedings of the International Conference of Nuclear Structure at High Angular Momentum, Ottawa, (1992), and AECL Report No. 10613 (unpublished), Vol. 2, p. 94.
[6] J. Thomson *et al.*, Phys. Rev. **C81**, 014307 (2010).
[7] K. Lagergren *et al.*, Phys. Rev. **C83**, 014313 (2011).
[8] J.M. Rees *et al.*, Phys. Rev. **C83**, 044314 (2011).
[9] M.C. Drummond *et al.*, Phys. Rev. **C87**, 054309 (2013).
[10] H.J. Li *et al.*, Phys. Rev. **C92**, 014326 (2015).
[11] C.W. Beausang and J. Simpson, J. Phys. **G22**, 527 (1996).
[12] C.W. Beausang *et al.*, Nucl. Instrum. and Meth. in Phys. Res. **A313**, 37 (1992).
[13] M. Leino *et al.*, Nucl. Instrum. and Meth. in Phys. Res. **B99**, 653 (1995).
[14] R.D. Page *et al.*, Nucl. Instrum. and Meth. in Phys. Res. **B204**, 634 (2003).
[15] I.H. Lazarus *et al.*, IEEE Transactions on Nuclear Science **48** 567 (2001)
[16] P. Rahkila, Nucl. Instrum. and Meth. in Phys. Res. **A595**, 637 (2008).
[17] D.C. Radford, Nucl. Instrum. and Meth. in Phys. Res. **A361**, 297 (1995).
[18] K.S. Krane, R.M. Steffen, and R.M. Wheeler, Nucl. Data Tables A **11**, 351 (1973).
[19] F.F. Hanna, Ph.D. Thesis, University of Liverpool, (1993).
[20] A.N. James *et al.*, Nucl. Instrum. and Meth. in Phys. Res. **A267** 144 (1988).
[21] A. Bohr and B. R. Mottelson, *Collective Nuclear Motion and the Unified Model* in Beta and Gamma Ray Spectroscopy. North Holland, Amsterdam, first edition, 1955.
[22] M. Sandzelius *et al.*, Phys. Rev. **C80**, 054316 (2009).
[23] K.-H. Schmidt *et al.*, Phys. Lett. **B168**, 39 (1986).
[24] R. S. Simon *et al.*, Z. Phys. **A125**, 197 (1986).
[25] E.S. Paul *et al.*, Phys. Rev. **C51**, 78 (1995).
[26] S. Hofmann *et al.*, Z. Phys. **A**291, 53 (1979).
[27] S. Hofmann, G. Münzenberg, F.P. Hessberger, W. Reisdorf, P. Armbruster, and B. Thuma, Z. Phys. **A299**, 281 (1981).
[28] R.D. Page *et al.*, Phys. Rev. **C53**, 660 (1996).
[29] A. Rytz *et al.*, At. Data Nucl. Data Tables **47**, 205 (1991).
[30] S. Cwiok, J. Dudek, W. Nazarewicz, W. Skalsi, and T. Werner, Comput. Phys. Commun. **46**, 379, (1987).
[31] R. Wyss, J. Nyberg, A. Johnson, R. Bengtsson, and W. Nazarewicz, Phys. Lett. **B215**, 211 (1988).
[32] R. Bengtsson, S. Frauendorf, and F.R. May, At. Data Nucl. Data Tables **35**, 15 (1986).
[33] I. Hamamoto, J. Höller, and X.Z. Zhang, Phys. Lett. **B226**, 17 (1989).
[34] M.A. Riley *et al.*, Nucl. Phys. **A486**, 456 (1986).
[35] D.C. Radford *et al.*, Nucl. Phys. **A545**, 365 (1992).
[36] J. Simpson *et al.*, J. Phys. **G13**, 847 (1987).
[37] J.N. Mo *et al.*, Nucl. Phys. **A472**, 295 (1987).
[38] D.T. Joss *et al.*, Phys. Rev. **C68**, 014303 (2003).
[39] P.A. Butler and W. Nazarewicz, Rev. Mod. Phys. **68**, 349 (1996).